Machine learning-based prediction of CFST columns using gradient tree boosting algorithm

Quang-Viet Vu [a], Viet-Hung Truong [b,*], Huu-Tai Thai [c]

[a] Faculty of Civil Engineering, Vietnam Maritime University, 484 Lach Tray Street, Haiphong City, Viet Nam
[b] Faculty of Civil Engineering, Thuyloi University, 175 Tay Son, Dong Da, Hanoi, Viet Nam
[c] Department of Infrastructure Engineering, The University of Melbourne, Parkville, VIC 3010, Australia

ARTICLE INFO

ABSTRACT

Among recent artificial intelligence techniques, machine learning (ML) has gained significant attention during the past decade as an emerging topic in civil and structural engineering. This paper presents an efficient and powerful machine learning-based framework for strength predicting of concrete filled steel tubular (CFST) columns under concentric loading. The proposed framework was based on the gradient tree boosting (GTB) algorithm which is one of the most powerful ML techniques for developing predictive models. A comprehensive database of over 1,000 tests on circular CFST columns was also collected from the open literature to serve as training and testing purposes of the developed framework. The efficiency of the proposed framework was demonstrated by comparing its performance with that obtained from other ML methods such as random forest (RF), support vector machines (SVM), decision tree (DT) and deep learning (DL). The accuracy of the developed predictive model was also verified with the current design equations from modern codes of practice as well as existing ML-based predictive models.

1. Introduction

Machine learning (ML) is one of the most promising artificial intelligence (AI) techniques that has been increasingly used for modelling and predicting the behavior of problems in civil engineering [1–3] and structural engineering [4–9] in recent years. Different ML algorithms such as random forest (RF), artificial neural network (ANN), decision tree (DT), support vector machines (SVM), deep learning (DL) and gradient tree boosting (GTB) have been developed. Within the structural engineering domain, ANN is the most commonly used method to predict compressive strength and modulus of concrete [10–19], time-dependent properties of structures [20–29], bond strength FRP and concrete [30], the strength of concrete slabs [31,32], and the fire resistance [33] and ultimate strength [34–45] of concrete-filled steel tubular (CFST) columns. The GBT algorithm, however, is considered as the most robust and powerful DL method which can be trained faster and more accurate than other existing ML methods [46–50]. It is therefore used in this study to develop predictive models for CFST columns.

CFST columns are one of the most efficient structural members in terms of structural performance and construction cost because of utilizing the merits of both structural steel and concrete materials [51].

The economic benefits of such CFST columns can be significantly enhanced in high-rise building applications if high strength materials are used because their member size can be reduced by half compared with normal strength materials [52–54]. In the current codes of practice, however, the design guidelines for CFST columns are redistricted to a certain limit of material strength as shown in Table 1. For example, both European code EC 4 [55] and British code BS 5400 [56] are limited the use of concrete compressive strength to 50 MPa, whilst this limit is slightly increased up to 70 MPa in American code AISC 360-16 [57] and Chinses code GB 50936 [58]. Japanese code AIJ [59] and Australian/New Zealand code ASNZS 2327 [60] are the only two codes that allow high strength concrete with the compressive strength up to 90 MPa and 100 MPa, respectively. However, these limits are far behind the current development of high strength concrete with the compressive strength up to 200 MPa [61].

With recent advent of ML techniques and the availability of test database, it is possible to develop alternatively ML-based predictive model to overcome the limit of current design equations. Existing empirical formulas for strength prediction of CFST columns also exhibit certain limits. For example, Wang et al. [62] proposed an empirical equation for high-strength CFST columns with concrete compressive

---

* Corresponding authors.
E-mail addresses: vietvq@vimaru.edu.vn (Q.-V. Vu), truongviethung@tlu.edu.vn (V.-H. Truong), tai.thai@unimelb.edu.au (H.-T. Thai).

Table 1
Material limits in current design codes for CFST columns.

Design codes	Steel yield stress (MPa)	Concrete strength (MPa)
AISC 360-16 [57]	525	69
EC 4 [55]	460	50
BS 5400 [56]	460	50
GB 50936 [58]	420	70
AIJ [59]	440	90
ASNZS 2327 [60]	690	100*

* The updated version published on June 2020 allows up to 120 MPa.

strength and steel yield stress up to 120 MPa and 960 MPa, respectively. However, their equation is only applied for the stub column. The ANN-based predictive model proposed by Tran et al. [63] was limited to CFST columns with concrete strength of 113 MPa. However, their equation was derived base on a small number of test data, and thus resulting less accuracy.

This paper aims to develop an efficient ML-based framework for predicting the strength of circular CFST columns under concentric loading using the GBT algorithm. To assess the performance of the developed model, the K-fold cross-validation method associated with three indicators of mean square error (MSE), coefficient of determination R-squared (R2), and adjusted coefficient of determination (adjusted R2) were utilized. A test database composed of 1,017 specimens on circular CFST columns was collected for training and testing purposes of the developed framework. Four different ML models composed of SVM, RF, DT, and DL were used to demonstrate the efficiency of the developed framework. The accuracy of the developed predictive model was also verified with the current design equations and existing predictive models.

2. Review of design models of circular CFST columns

For the sake of comparison, this section will briefly summarize the design equations from current codes of practice. Two most accurate existing models developed by Wang et al. [62] and Tran et al. [63] were also adopted to demonstrate the accuracy of the proposed framework. It is noted that the same notations were employed for similar terms in each design equation for the sake of consistency (e.g., member strength, cross-section strength, relative slenderness).

2.1. EC 4 formula

For circular CFST sections, the equation to calculate its axial compressive strength is expressed as follows [55]

$$P_{uc}^{EC4} = \chi P_{us}^{EC4} = \chi \left[A_s f_y \eta_s + A_c f_c' \left(1 + \eta_c \frac{t}{D} \frac{f_y}{f_c'} \right) \right] \tag{1}$$

where

$$\eta_s = \eta_{s0} + (1 - \eta_{s0}) \frac{10e}{D} \tag{2}$$

$$\eta_c = \eta_{c0} \left(1 - \frac{10e}{D} \right) \tag{3}$$

$$\eta_{s0} = 0.25 \left(3 + 2 \bar{\lambda} \right) \leqslant 1 \tag{4}$$

$$\eta_{c0} = 4.9 - 18.5 \, \bar{\lambda} + 17 \bar{\lambda}^{-2} \geqslant 0 \tag{5}$$

$$\bar{\lambda}^{EC4} = \sqrt{\frac{N_{ns}}{N_{cr}}} \leqslant 0.5 \tag{6}$$

$$P_{ns} = A_s f_y + A_c f_c' \tag{7}$$

$$P_{cr}^{EC4} = \frac{\pi^2 (EI)_{eff}^{EC4}}{L_e^2} \tag{8}$$

$$(EI)_{eff}^{EC4} = E_s I_s + 0.6 E_c^{EC4} I_c \tag{9}$$

$$E_c^{EC4} = 22 \left[(f_c' + 8)/10 \right]^{0.3} \tag{10}$$

$$\chi = \frac{1}{\phi + \sqrt{\phi^2 - \bar{\lambda}^2}} \leqslant 1 \tag{11}$$

$$\phi = 0.5 \left[1 + 0.21 \left(\bar{\lambda} - 0.2 \right) + \bar{\lambda}^{-2} \right] \tag{12}$$

where η_s and η_c are the confining coefficients. η_{s0} and η_{c0} are the steel reduction and the concrete enhancement factors, respectively. $\bar{\lambda}$ is the relative slenderness. P_{ns} and P_{cr} are the squash and buckling strength, respectively. L_e is the column effective length and $(EI)_{eff}^{EC4}$ is the effective flexural stiffness. I_s and I_c are the second moments of area of the steel and concrete sections, respectively. E_c^{EC4} is the Young's modulus of concrete and χ is the global buckling reduction factor.

2.2. AISC 360–16 formula

Based on classification of its section slenderness, the section strength of circular CFST columns is computed in three cases. The section strength of compact sections is expressed as [57]

$$P_{us}^{AISC} = P_p = A_s f_y + 0.95 A_c f_c' \tag{13}$$

For non-compact sections, the section strength will be interpolated between the compact strength P_p and yield strength P_y as

$$P_{us}^{AISC} = P_p - \frac{P_p - P_y}{(\lambda_r - \lambda_p)^2} (\lambda - \lambda_p)^2 \tag{14}$$

$$\lambda_p = 0.09 \frac{E_s}{f_y} \tag{15}$$

$$\lambda_r = 0.19 \frac{E_s}{f_y} \tag{16}$$

$$P_y = A_s f_y + 0.7 A_c f_c' \tag{17}$$

The section strength of slender sections is computed as

$$P_{us}^{AISC} = A_s f_{cr} + 0.7 A_c f_c' \tag{18}$$

$$f_{cr} = \frac{0.72 f_y}{\left(D f_y / E_s t \right)^{0.2}} \tag{19}$$

The member strength is determined as

$$P_{uc} = \begin{cases} P_{us} \left(0.658^{\frac{N_{us}}{N_{cr}}} \right) & \text{if } \frac{P_{us}}{P_{cr}} \leqslant 2.25 \\ 0.877 N_{cr} & \text{if } \frac{P_{us}}{P_{cr}} > 2.25 \end{cases} \tag{20}$$

$$P_{cr}^{AISC} = \frac{\pi^2 (EI)_{eff}^{AISC}}{L_e^2} \tag{21}$$

$$(EI)_{eff}^{AISC} = E_s I_s + C_3 E_c^{AISC} I_c \tag{22}$$

$$C_3 = 0.45 + 3 \frac{A_s}{A_s + A_c} \leqslant 0.9 \tag{23}$$

$$E_c^{AISC} = 0.043 \rho_c^{1.5} \sqrt{f_c'} \tag{24}$$

2.3. ASNZS 2327 formula

In a similar format with EC 4, the section predicted by ASNZS 2327 [60] is in the following form

$$P_{us}^{AS} = k_f A_s f_y \eta_s + A_c f_c' \left(1 + \eta_c \frac{t}{D} \frac{f_y}{f_c'}\right) \tag{25}$$

$$D_e = \min\left(D\sqrt{\frac{\lambda_{ey}}{\lambda_e}}, D\left(\frac{3\lambda_{ey}}{\lambda_e}\right)^2\right) \leqslant D \tag{26}$$

$$\lambda_{ep} = 2.26\sqrt{\frac{E_s}{f_y}} \tag{27a}$$

$$\lambda_{ey} = 3\sqrt{\frac{E_s}{f_y}} \tag{27b}$$

$$A_e = \pi\left(D_e t - t^2\right) \tag{28}$$

$$\overline{\lambda}^{AS} = \sqrt{\frac{N_{us}}{N_{cr}}} \tag{29}$$

$$P_{ns} = k_f A_s f_y + A_c f_c' \tag{30}$$

$$P_{cr}^{AS} = \frac{\pi^2 (EI)_{eff}^{AS}}{L_e^2} \tag{31}$$

$$(EI)_{eff}^{AS} = E_s I_s + E_c^{AS} I_c \tag{32}$$

$$E_c^{AS} = \begin{cases} \rho_c^{1.50} 0.043\sqrt{f_{cmi}} & \text{if } f_{cmi} \leqslant 40MPa \\ \rho_c^{1.5}\left(0.024\sqrt{f_{cmi}} + 0.12\right) & \text{if } f_{cmi} > 40MPa \end{cases} \tag{33}$$

$$f_{cmi} = 0.9\left(1.2875 - 0.001875 f_c'\right) f_c' \tag{34}$$

The ultimate load-carrying capacity of CFST columns is then given by

$$P_{uc}^{AS} = \alpha_c P_{us} \tag{35}$$

$$\alpha_c = \xi\left[1 - \sqrt{1 - \left(\frac{90}{\xi\lambda}\right)^2}\right] \tag{36}$$

$$\xi = \frac{\left(\frac{\lambda}{90}\right)^2 + 1 + \eta}{2\left(\frac{\lambda}{90}\right)^2} \tag{37}$$

$$\lambda = \lambda_\eta + \alpha_a \alpha_b \tag{38}$$

$$\eta = 0.00326(\lambda - 13.5) \geqslant 0 \tag{39}$$

$$\lambda_\eta = 90\,\overline{\lambda} \tag{40}$$

$$\alpha_a = \frac{2100(\lambda_\eta - 13.5)}{\lambda_\eta^2 - 15.3\lambda_\eta + 2050} \tag{41}$$

$$\alpha_b = \begin{cases} 0 \text{ if } k_f < 1 \\ 1 \text{ if } k_f = 1 \end{cases} \tag{42}$$

in which the local buckling factor k_f is calculated as the ratio of the effective area (excluding the local buckling part) to the gross area of the steel tube. D_e and A_e are the effective diameter and effective area for circular sections, respectively. f_{cmi} is the mean value of the in-situ compressive concrete strength. α_c is the member slenderness reduction factor.

2.4. Wang's formula

The strength of the circular CFST columns proposed by Wang et al. [62] is given as

$$P^{Wang} = \eta_a f_y A_s + \eta_c f_c' A_c \tag{43}$$

$$\eta_a = 0.95 - 12.6 f_y^{-0.85} \ln(0.14D/t) \tag{44}$$

$$\eta_c = 0.99 + \left[5.04 - 2.37(D/t)^{0.04}(f_c')^{0.1}\right]\left(tf_y/Df_c'\right)^{0.51} \tag{45}$$

in which A_c and A_s are respectively the areas of infilled concrete and the steel tube. f_c' and f_y are the compressive strength of the concrete infill and the yield stress of the steel tube, respectively. D and t are respectively the outer diameter and the thickness of the steel tube. η_c and η_a are respectively the confining factor of the infilled concrete and the steel tube which are similar to the cases of EC 4 and ASNZS 2327.

2.5. Tran's formula

Based on proposed ANN model, Tran et al. [63] established an equation to compute the axial compressive strength of circular CFST columns as given by

$$P_u = (P_u)_{chart} C_L C_t C_{f_y} C_{f_c'} \tag{46}$$

$$C_L = 0.0006\left(\frac{L}{600}\right)^2 - 0.0660\left(\frac{L}{600}\right) + 1.0650 \tag{47}$$

$$C_t = -0.0792\left(\frac{t}{5}\right)^3 + 0.2540\left(\frac{t}{5}\right)^2 + 0.2770\left(\frac{t}{5}\right) + 0.5497 \tag{48}$$

$$C_{f_y} = 0.0701\left(\frac{f_y}{350}\right)^2 + 0.1114\left(\frac{f_y}{350}\right) + 0.8164 \tag{49}$$

$$C_{f_c'} = -0.0539\left(\frac{f_c}{50}\right)^3 + 0.1058\left(\frac{f_c}{50}\right)^2 + 0.5518\left(\frac{f_c}{50}\right) + 0.3963 \tag{50}$$

$$(P_u)_{chart} = 0.0462D^2 + 4.7889D + 88.876 \tag{51}$$

where C_L, C_t, C_{Fy}, $C_{fc'}$ are the derive correction factors. $(P_u)_{chart}$ is the axial compressive strength of circular CFST column at reference parametric values.

3. Collected experimental dataset

For the training and testing purpose of the developed ML-based framework, a total of 1,017 tests on circular CFST subjected to uniaxial compression was collected based on the database collected by Thai et al. [64] in addition to the recent tests published in 2020. Detailed properties and test results for each specimen of this database can be found in Thai et al. [65]. A summary of the ranges of geometric and material parameters of the test database was shown in Table 2. The values of outer diameter (D), steel tube thickness (t), column length (L), concrete compressive strength (f_c') and steel yield stress (f_y) of the specimens are in the range of 44.5 mm–1020 mm, 0.52 mm–16.54 mm, 152.4 mm–5560 mm, 7.6 MPa–185.9 MPa and 178.3 MPa–853 MPa, respectively.

The histograms of the dataset corresponding to D, t, f_y, f_c', and L were presented in Fig. 1. It is worth noting that most of the tests on the circular CFST columns were carried out using normal strength materials (91.84% data with $f_y \leqslant 460$ MPa and 76.2% data with $f_c' \leqslant 50$ MPa. Only a small amount of tests was conducted on high strength materials (8.16% data with $f_y > 460$ MPa, 14.46% data with 50 MPa $< f_c' \leqslant 90$ MPaand 9.34% data with $f_c' > 90$ MPa. In addition, it can be seen that most test specimens were made by compact and

Table 2
Statistical properties of experimental dataset.

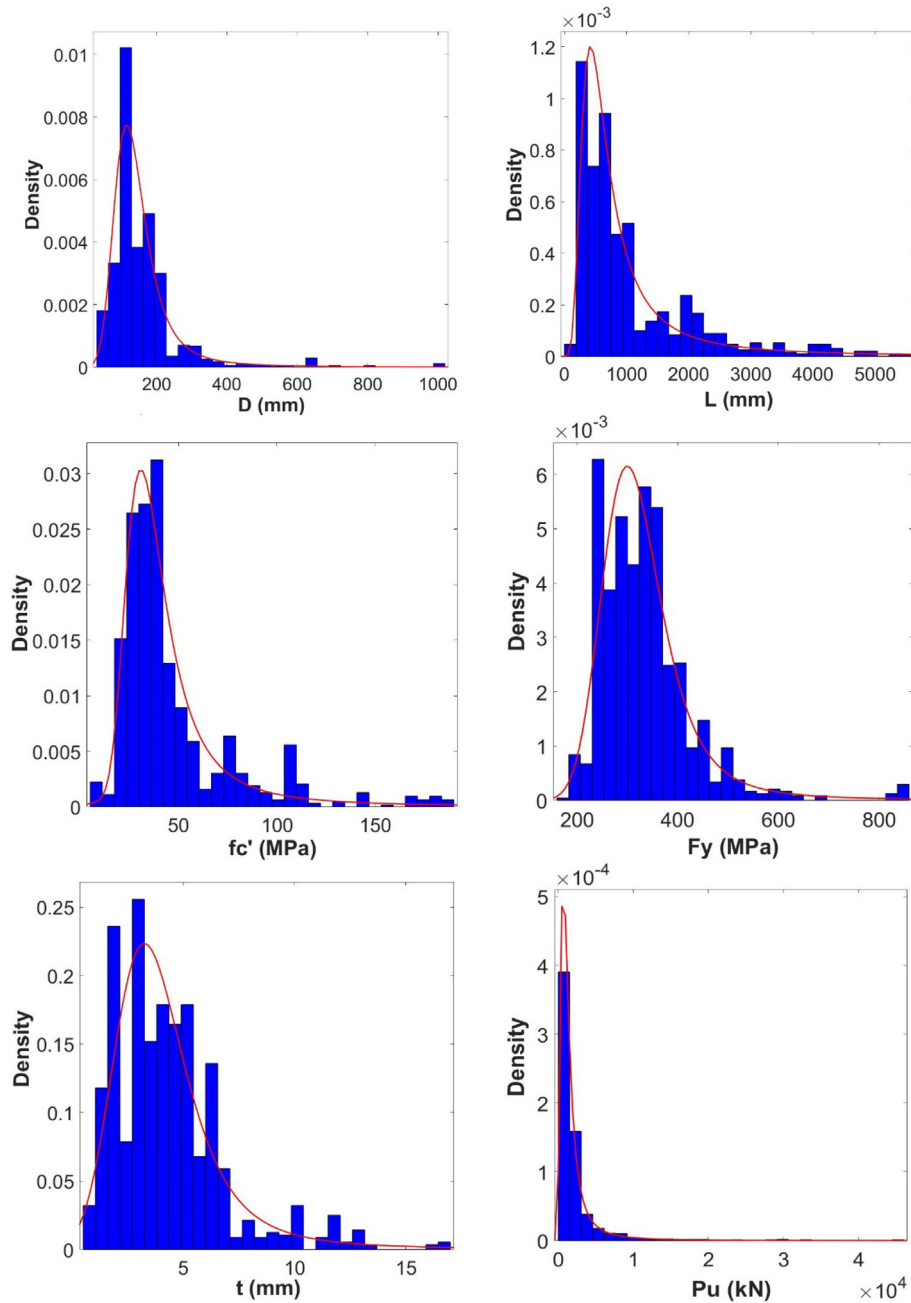| Input network	D(mm)	t (mm)	f_y (MPa)	f_c' (MPa)	L (mm)	P_u (MPa)
Maximum	1020	16.54	853	185.94	5560	46,000
Minimum	44.5	0.52	178.28	7.59	152.35	45
Mean	127.1	4	324	37.49	700	1210
Standard deviation	109.78	2.55	93.99	30.68	981.49	4175.47

Fig. 1. Histogram of the test database.

non-compact sections, whilst the number of test specimens made by slender sections was very limited.

4. Proposed ML-based predictive model

It is well-known that the formula presented in Section 2 were formulated based on the experimental data. Obviously, the reliability of the developed formula is dependent on two main factors: (1) the number of experimental data and (2) the error between the formula and the experimental tests. To satisfy the first factor, over 1,000 experimental data were collected in Section 3 which can be considered as the most comprehensive and up-to-date database having been collected in the open literature. To account for the second factor, instead of proposing new formula as previous works, a GTB-based metamodel was developed in this study. Since the metamodel developed by minimizing the error between the predicted values and test results has a

highly complicated structure compared to formula, it can show more accurately the relationship between the input and output data. In this section, the basic algorithm of GTB will be presented first, and then the framework of the proposed method for CFST columns will be introduced. The detail is as following.

4.1. GTB algorithm

The GTB method was developed by Friedman in 1999 [66]. To better understand the GTB algorithm, we considered the vector input $X = \{x_1, ..., x_n\}$ with its output y. A metamodel represented by the function $F_{opt}(X)$ can be defined as the loss function $Loss(y, F(X))$ between the predicted values $F(X_i)$ and exact results y_i as

$$F_{opt}(X) = \underset{F(X)}{\mathrm{argmin}}\, Loss(y, F(X)) \tag{52}$$

Fig. 2 presented a tree ensemble model to solve the optimization problem presented in Eq. (52). As can be seen in this figure, several decision trees (base learner) are developed in a sequential fashion where the residual of the current decision tree is the output of the next one. In this way, the high error of a decision tree can be reduced step by step in the tree ensemble model. The GTB method is also a type of the tree ensemble models in which a subsample of the train data at each iteration is randomly taken from the full train data. This subsample will be then employed to fit the base learner and update the model for the next iteration. In the GTB method, the output is computed as

$$F(X) = \sum_{m=0}^{M} \beta_m f(X; a_m) \tag{53}$$

where $\{\beta_m\}_0^M$ is used to perform the importance of the base learners, and $f(X; a_m)$ is a mathematical function chosen for the base learner m^{th}. For simplicity, $f(X; a_m)$ was taken as a simple function of X as follow

$$f(X; a_m) = a_m^T X \tag{54}$$

where $a_m = \{a_1^m, a_2^m, ..., a_n^m\}$ are calculated by using an optimization process to minimize the error of the corresponding decision tree. By using an initial guess $F_0(X) = \underset{\gamma}{\mathrm{argmin}} \sum_{i=1}^{N} Loss(y_i, \gamma)$, the model can be updated as follow

$$F_m(X) = F_{m-1}(X) + \beta_m f(X; a_m) \tag{55}$$

A two-step gradient decent-like procedure was adopted to calculate β_m and a_m. In the first step, a_m is determined as
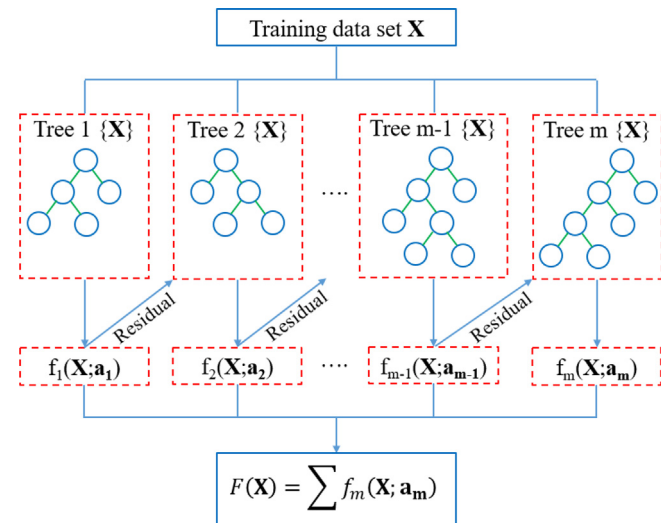
$$a_m = \underset{a,\rho}{\mathrm{argmin}} \sum_{i=1}^{N} \left[\tilde{y}_{im} - \rho f(X_i; a) \right]^2 \tag{56}$$

$$\tilde{y}_{im} = - \left[\frac{\partial Loss(y_i, F(X_i))}{\partial F(X_i)} \right]_{F(X)=F_{m-1}(X)} \tag{57}$$

in which ρ is the step size. In the second step, β_m is determined as

$$\beta_m = \underset{\beta}{\mathrm{argmin}} \sum_{i=1}^{N} Loss(y_i, F_{m-1}(X_i) + \beta f(X_i; a_m)) \tag{58}$$

At iteration m, the X space is assumed to be divided into L-disjoint regions $\{R_{lm}\}_{l=1}^{L}$, and thus the constant value of each region can be determined as

$$f(X, \{R_{lm}\}_{l=1}^{L}) = \sum_{l=1}^{L} \bar{y}_{lm} I(X \in R_{lm}) \tag{59}$$

where $I(X \in R_{lm}) = \begin{cases} 1 & if \ \ X \in R_{lm} \\ 0 & otherwise \end{cases}$ with $\bar{y}_{lm} = mean_{X_i \in R_{lm}} \left(\tilde{y}_{im} \right)$. Since Eq. (59) predicts the output values for the regions R_{lm}, Eq. (58) can be written as

$$\gamma_{lm} = \underset{\gamma}{\mathrm{argmin}} \sum_{X_i \in R_{lm}} Loss(y_i, F_{m-1}(X_i) + \gamma) \tag{60}$$

Eq. (55) is then rewritten as

$$F_m(X) = F_{m-1}(X) + \nu \cdot \gamma_{lm} I(X \in R_{lm}) \tag{61}$$

where ν is the "shrinkage" parameter which is used to control the learning rate. It can be taken as $\nu \leqslant 0.1$ [66] for better performance.

4.2. Framework of proposed method

The GTB-based procedure for strength prediction of CFST columns was proposed as follow.

Step 1: Dataset and scale

Dataset collected in Section 3 will be divided into two groups of training (X_{train}, Y_{train}) and testing (X_{test}, Y_{test}). Data will then be scaled down in the range [0,1]. It should be note that the GTB does not require data scaling. However, in this study, several ML methods are used for comparison to demonstrate the performance of the GTB. Therefore, data scaling is required for comparison purpose as follow

$$x_i^{scale} = \frac{x_i}{x_i^{max}} \tag{62a}$$

$$y^{scale} = \frac{y_i}{y_i^{max}} \tag{62b}$$

where x_i^{max} is the maximum value of the input x_i of the dataset and y_{max} is the maximum value of the output data.

Step 2: Define a training model

The GTB predictive model will have the following four main components including (i) the loss function, (ii) DT definition, (iii) number of boosting stages, and (iv) learning rate. Description of each component can also be found in Truong et al. [47].

Step 3: Train the GTB model defined in Step 2

Before the GTB model can be used for CFST columns, it needs to be trained using the training dataset prepared in Step 1.

5. Results and discussion

5.1. Performance of the proposed method

The dataset is divided into 20% testing data and 80% training data [47]. Three indicators of MSE, R^2, and adjusted R^2 ($\bar{R}^2$) were used to evaluate the performance of the proposed GTB model.

Fig. 2. Illustration of the tree ensemble model.

$$MSE = \frac{\sum_{i=1}^{m}(P_i - T_i)^2}{m} \qquad (63)$$

$$R^2 = 1 - \frac{\sum_{i=1}^{m}(P_i - T_i)^2}{\sum_{i=1}^{m}\left(T_i - \bar{T}\right)^2} \qquad (64)$$

$$\bar{R}^2 = 1 - (1 - R^2)\left[\frac{n-1}{n-(k+1)}\right] \qquad (65)$$

in which T_i and P_i stand for the tested and predicted values, respectively; m is the total number of samples; k is the number of independent variables in the regression equation; and $\bar{T}$ denotes the mean value of all the tested values. Fig. 3 showed the comparison between the actual tested results and those predicted from the GTB model for 20% testing data (equivalent to 217 specimens). A very good agreement was obtained. The performance of the developed GTB model was demonstrated in Figs. 4, 5 and 6 for all data, training data, and testing data, respectively. It is apparent that the developed GTB model can give a very good prediction of all datasets. It is also noting worthy that the relationship between the predicted and actual data is very close to the unity line $y = x$ with very good distribution of the error of the predicted results (Fig. 5).

To investigate the effect of the input parameters consisting of D, t, f_c', L, and F_y on the strength prediction of CFST columns, a sensitivity analysis was performed. It can be observed from Fig. 7 that the outer diameter of the steel tube D plays the most critical role, and it is also the most dominant input parameter compared with the rest four input parameters which somehow have a similar level of importance to each other. This is expected because the outer tube diameter D is the main contributor to the cross-sectional area of CFST columns.

5.2. Performance comparison with other ML algorithms

The performance of the proposed GBT-based framework will be demonstrated in this section by comparing with other ML methods including SVM, RF, DT and DL. To minimize the bias between random
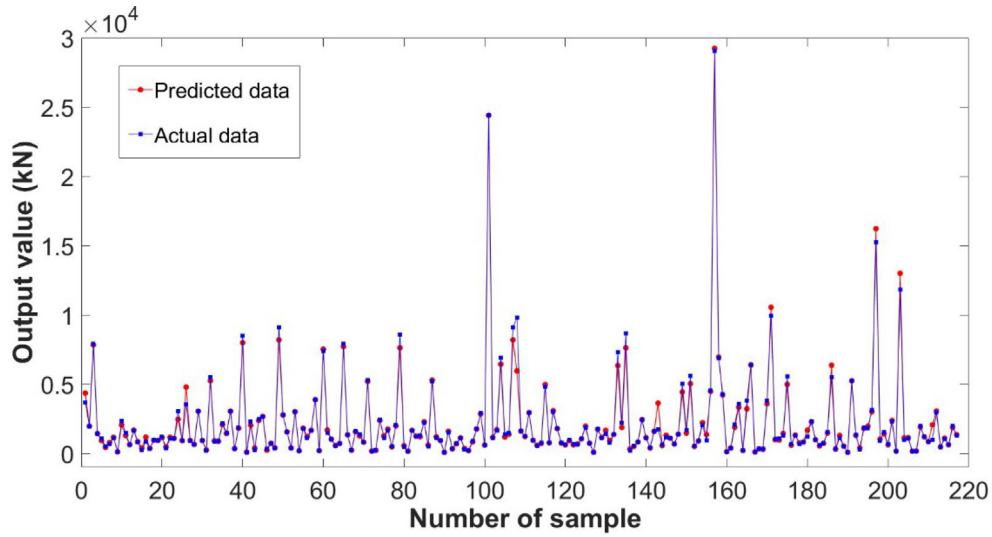

Fig. 3. Actual and predicted results from the GTB model for testing data.
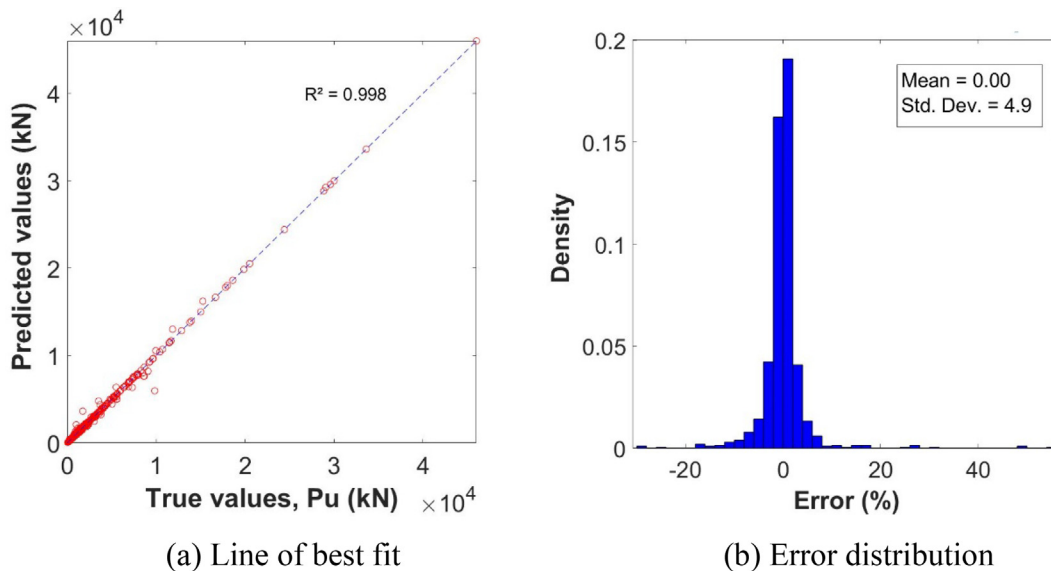

(a) Line of best fit

(b) Error distribution

Fig. 4. Predicted performance obtained from the GTB model for all data.

sample and training dataset, the 10-fold method was adopted. The 10-fold divides the dataset into ten subsets in which nine subsets are used to build up the strong learner, whilst the remaining subset is employed for validating the model. All parameters of the considered ML methods were refereed from Truong et al. [47] except for a network of *5-20-20-1* and a combining *model checkpoint and early stopping with number epoch of 500* adopted in this study for DL method.

Fig. 8 showed the comparison the accuracy of different models. It can be observed that all five ML methods give very high accuracy in prediction. Among them, the GTB model provided the best performance with the smallest error as shown in Table 3. The RF method gave the largest MSE, whilst the DT method gave the smallest R2. It is also noting worthy that the accuracy of the DL model is lower than that of the GTB model. In terms computational cost, Table 3 indicated that the DL model requested the longest running time among five ML methods, whilst the GTB model requested an average running time among these methods. Although the DT model gave the lowest running time, it yielded the least efficiency. It is noted that the running time

presented in Table 3 was the time for running one analysis. Based on the above observation, it can be concluded that the GTB model is the best efficiency among five ML methods.

5.3. Accuracy comparison with existing design equations and models

To show the accuracy of the developed GBT model, the obtained predictions were compared with those predicted by the current design codes of practice (i.e., EC 4, AISC 360-16 and ASNZS 2327) and those predicted the empirical developed by Wang et al. [62] and the ANN-based model developed by Tran et al. [63]. The equations for these models are also summarized in Section 2 for the sake of completeness.

Fig. 9 showed the comparison of the predictions obtained from various existing models. The error distribution of all compared models was also plotted in Fig. 10 as well as summarized in Tables 4 and 5 for testing data and all data, respectively. It should be noted that in the previous comparison reported by Tran et al. [63], the testing data was not considered in the comparison study. Therefore, it did not

(a) Line of best fit   (b) Error distribution
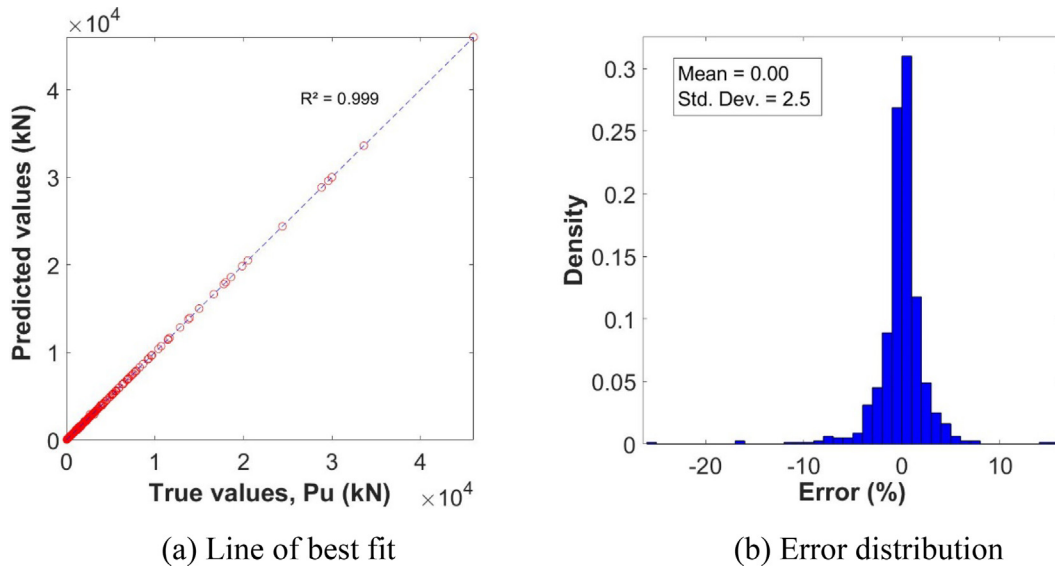
Fig. 5. Predicted performance obtained from the GTB model for training data.

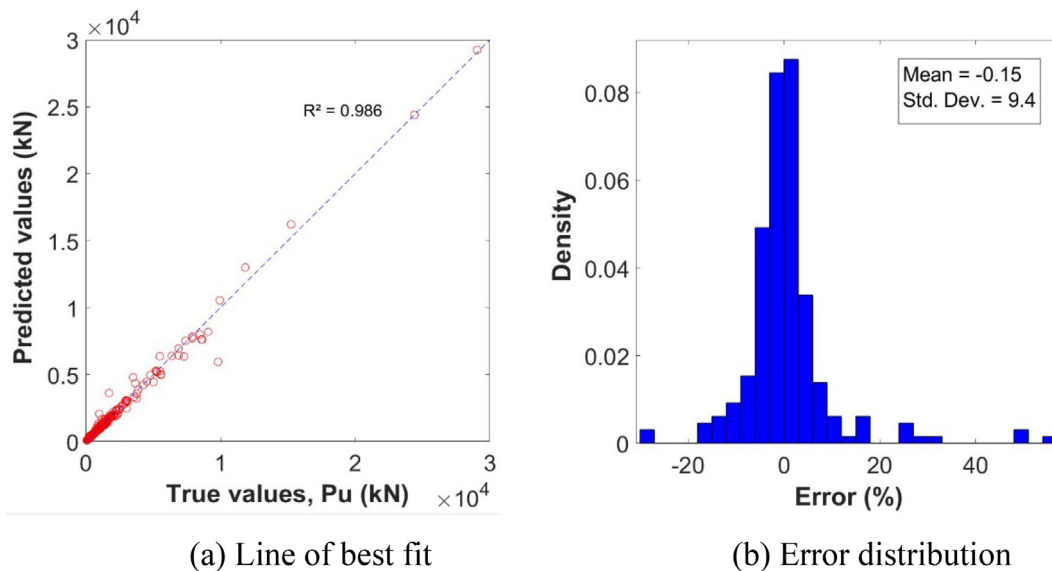(a) Line of best fit   (b) Error distribution

Fig. 6. Predicted performance obtained from the GTB model for testing data.
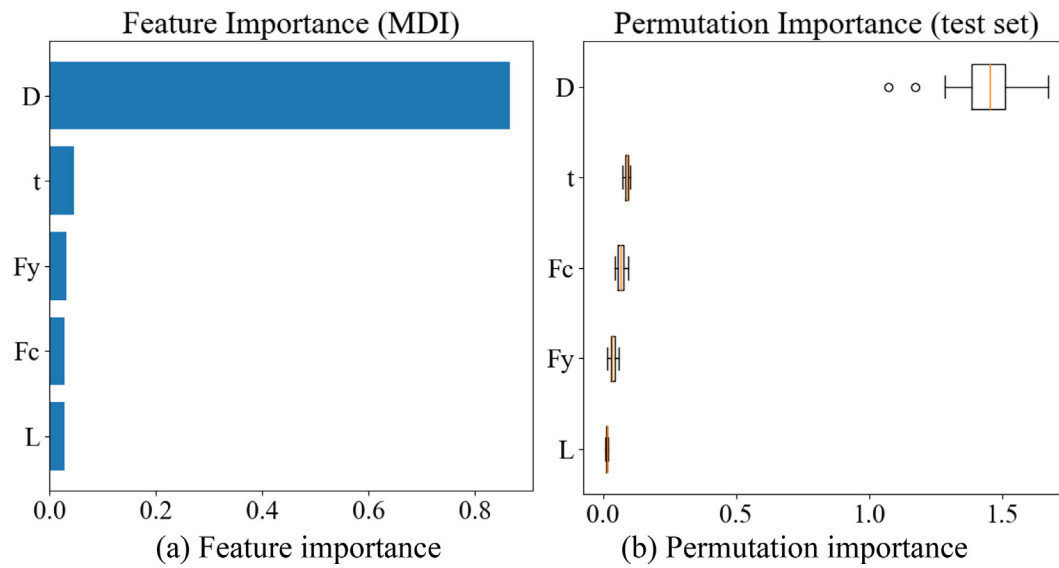
Fig. 7. Sensitivity analysis of input parameters.

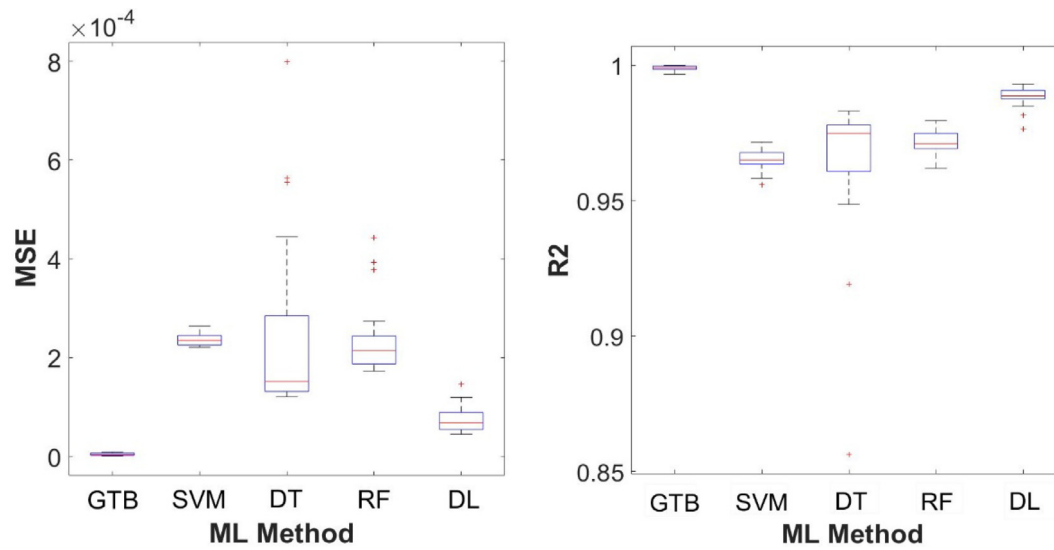

Fig. 8. Boxplot for accuracy different models.

Table 3
Comparison of the test data accuracy for different models.

Time analysis	GTB			SVM			DT			RF			DL		
	MSE	R^2	$\bar{R}^2$	MSE	R^2	$\bar{R}^2$	MSE	R^2	$\bar{R}^2$	MSE	R^2	$\bar{R}^2$	MSE	R^2	$\bar{R}^2$
No. 1	1.73E-06	0.9995	0.9995	2.25E-04	0.9680	0.9664	1.77E-04	0.9734	0.972	2.15E-04	0.9696	0.968	7.73E-05	0.9885	0.9879
No. 2	2.58E-06	0.9966	0.9964	2.33E-04	0.9634	0.9614	1.31E-04	0.9782	0.977	2.24E-04	0.9697	0.9681	6.63E-05	0.9863	0.9856
No. 3	8.12E-06	0.9992	0.9991	2.35E-04	0.9599	0.9578	1.23E-04	0.9831	0.9822	2.33E-04	0.9721	0.9707	1.20E-04	0.9815	0.9805
No. 4	5.89E-06	0.9977	0.9976	2.60E-04	0.9616	0.9596	1.21E-04	0.9809	0.9799	2.22E-04	0.9692	0.9675	4.51E-05	0.9930	0.9926
No. 5	8.04E-06	0.9982	0.9981	2.24E-04	0.9696	0.9680	4.45E-04	0.9486	0.9459	1.84E-04	0.9706	0.969	1.47E-04	0.9764	0.9751
No. 6	2.62E-06	0.9997	0.9997	2.21E-04	0.9715	0.9700	7.99E-04	0.8562	0.8487	4.43E-04	0.9628	0.9609	5.37E-05	0.9905	0.9900
No. 7	3.50E-06	0.9985	0.9984	2.60E-04	0.9650	0.9632	1.23E-04	0.9764	0.9752	1.73E-04	0.9795	0.9785	5.43E-05	0.9924	0.9920
No. 8	1.39E-06	0.9998	0.9997	2.35E-04	0.9666	0.9649	1.39E-04	0.9765	0.9753	3.78E-04	0.9677	0.966	9.64E-05	0.9860	0.9853
No. 9	7.01E-06	0.9991	0.999	2.25E-04	0.9668	0.9650	1.50E-04	0.973	0.9716	1.89E-04	0.9745	0.9732	1.08E-04	0.9901	0.9896
No. 10	1.46E-06	0.9999	0.9999	2.26E-04	0.9677	0.9660	2.11E-04	0.9748	0.9735	1.90E-04	0.971	0.9695	7.69E-05	0.9879	0.9872
No. 11	1.88E-06	0.9997	0.9997	2.54E-04	0.9667	0.9650	1.52E-04	0.9696	0.968	2.74E-04	0.9699	0.9684	8.72E-05	0.9896	0.9891
No. 12	3.55E-06	0.9997	0.9997	2.64E-04	0.9559	0.9536	1.63E-04	0.9779	0.9768	2.02E-04	0.9734	0.972	4.54E-05	0.9924	0.9920
No. 13	2.83E-06	0.9995	0.9995	2.41E-04	0.9582	0.9560	5.55E-04	0.919	0.9148	1.77E-04	0.9771	0.976	4.63E-05	0.9886	0.9880
No. 14	3.91E-06	0.9997	0.9996	2.44E-04	0.9635	0.9615	1.28E-04	0.9753	0.974	2.18E-04	0.969	0.9674	5.86E-05	0.9913	0.9908
No. 15	5.40E-06	0.9978	0.9977	2.48E-04	0.9667	0.9649	1.95E-04	0.9531	0.9507	1.79E-04	0.9757	0.9745	5.72E-05	0.9905	0.9900
No. 16	1.93E-06	0.9992	0.9992	2.37E-04	0.9640	0.9621	3.90E-04	0.9633	0.9614	1.88E-04	0.9625	0.9605	7.56E-05	0.9848	0.9840

Table 3 (*continued*)

Time analysis	GTB			SVM			DT			RF			DL		
	MSE	R^2	$\bar{R}^2$	MSE	R^2	$\bar{R}^2$	MSE	R^2	$\bar{R}^2$	MSE	R^2	$\bar{R}^2$	MSE	R^2	$\bar{R}^2$
No. 17	7.05E-06	0.9988	0.9987	2.21E-04	0.9689	0.9673	1.32E-04	0.9803	0.9793	1.90E-04	0.9761	0.9749	9.83E-05	0.9886	0.9880
No. 18	5.10E-06	0.9989	0.9989	2.33E-04	0.9643	0.9625	1.47E-04	0.9795	0.9784	2.68E-04	0.972	0.9706	6.69E-05	0.9903	0.9898
No. 19	9.30E-06	0.9987	0.9986	2.40E-04	0.9678	0.9661	5.63E-04	0.9528	0.9503	1.86E-04	0.9768	0.9756	5.53E-05	0.9919	0.9914
No. 20	7.36E-06	0.9983	0.9982	2.34E-04	0.9643	0.9624	1.45E-04	0.9779	0.9768	3.93E-04	0.9619	0.9599	6.83E-05	0.9879	0.9873
Mean	4.53E-06	0.9989	0.9989	2.38E-04	0.9650	0.9632	2.50E-04	0.9635	0.9616	2.36E-04	0.9711	0.9696	7.52E-05	0.9884	0.9878
RunningTime (s)	36.12			27.32			4.76			68.73			430.3		

(a) Testing data

(b) All data
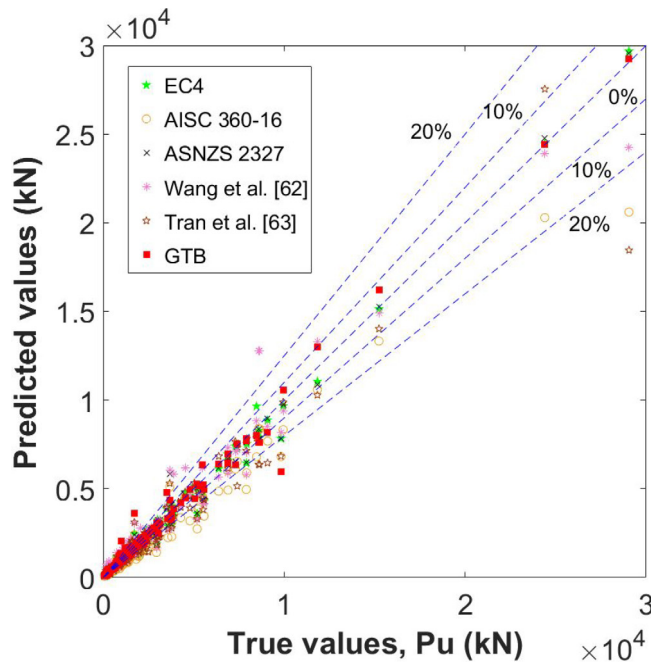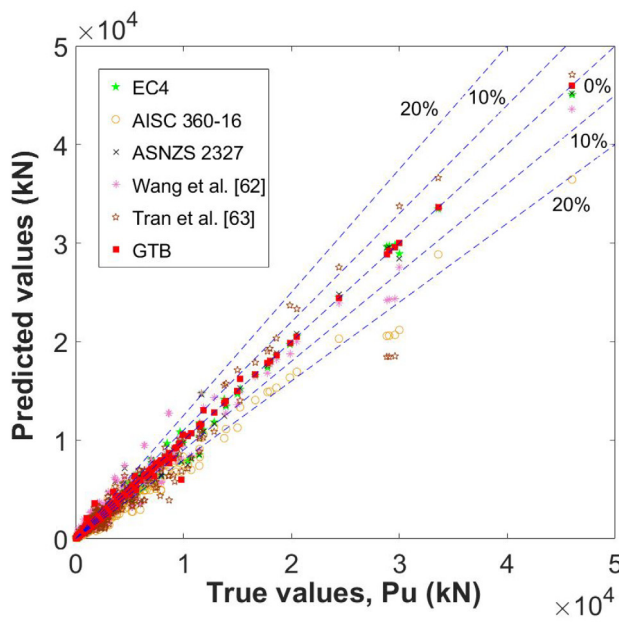
Fig. 9. Comparison between GTB model and the existing equations for testing data.

reflect the real accuracy of the model. The reason is that by comparison for all data, the accuracy of the model will be increased since the model accuracy of the training data is generally very high. This can be demonstrated when comparing the results between Tables 4 and 5 indicated that the accuracy of all models for all data is always higher than that for testing data. It can be seen that the accuracy of the proposed GBT-based predictive model is much higher than that of existing models especially in the range of a small error. For the large error range, the proposed GBT-based model only provided a slight improvement compared with existing models. For instance, for the error range of 5%, the accuracy of the proposed GBT model was 69.59% for testing data and 90.46% for all data. These values were almost three times better than those of existing models. Among three design codes considered, ASNZS 2327 provided the best prediction with the corresponding accuracy of 27.19% and 32.15%. These values were slightly higher than those of 22.12% and 30.97% of EC 4, but much better than those of 8.29% and 11.50% of AISC 360-16. The empirical equation proposed by Wang et al. [62] was more accurate than that of AISC 360-16, but was not comparable with EC 4 and ASNZS 2327. Meanwhile, the ANN-based model developed by Tran et al. [63] gave a low accuracy which was somehow similar to that of the empirical equation proposed by Wang et al. [62]. The reason was that the ANN-based model was built based on a limited number of test database with only 258 specimens, which was much smaller than 1,017 specimens used in this study. Therefore, it can be concluded that the proposed GTB-based model gives not only the best performance but also the best accuracy in predicting the strength of CFST columns.

6. Conclusions

An efficient and robust GTB-based method has been proposed in this study for strength prediction of circular CFST columns under concentric loading. The most comprehensive and up-to-date database with over 1,000 tests on circular CFST columns was also collected for testing and training the developed model. The performance of the developed model was demonstrated through the comparison with existing ML methods. The result indicated that the developed model was the most robust and powerful tool which could be trained faster and more accurate than other existing ML methods. The accuracy of the proposed model was also verified with existing design codes and models. The verification study showed the superior accuracy of the proposed model compared with existing design equations and models especially within the small error range.
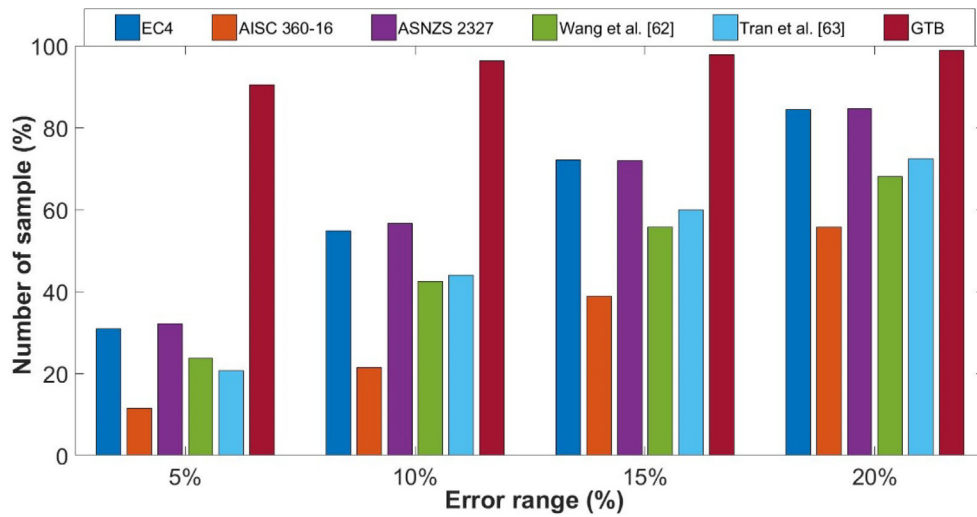
Declaration of Competing Interest

The authors declare that they have no known competing financial interests or personal relationships that could have appeared to influence the work reported in this paper.
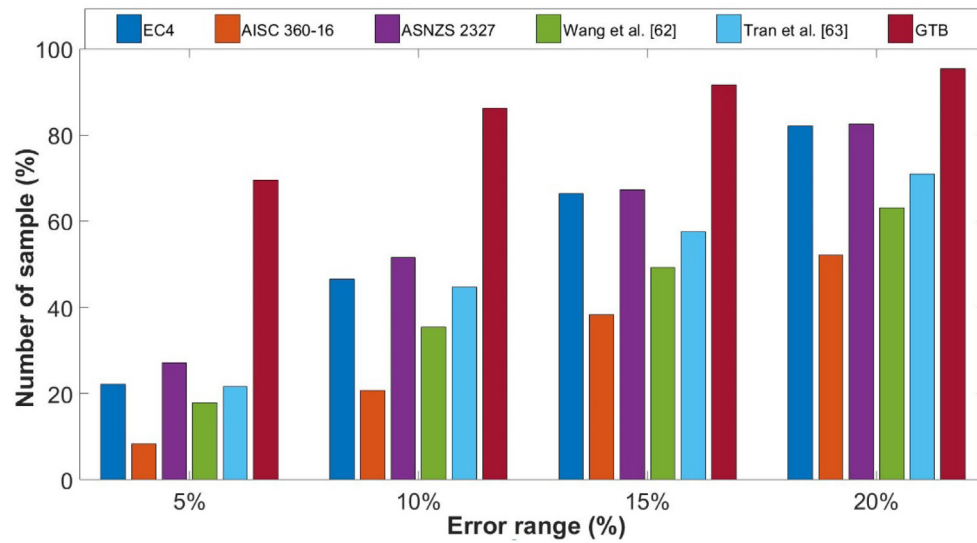
(a) Testing data

(b) All data

Fig. 10. Distribution of the error range.

Table 4
Error range distribution for testing data.

Error range (%)	Number of data and corresponding percentage in the error range					
	EC 4	AISC 360-16	ASNZS 2327	Wang et al. [62]	Tran et al. [63]	*GTB*
± 5	48 (22.12%)	18 (8.29%)	59 (27.19%)	39 (17.97%)	47 (21.66%)	151 (69.59%)
± 10	101 (46.54%)	45 (20.74%)	112 (51.61%)	77 (35.48%)	97 (44.70%)	187 (86.18%)
± 15	144 (66.36%)	83 (38.25%)	146 (67.28%)	107 (49.31%)	125 (57.60%)	199 (91.71%)
± 20	178 (82.03%)	113 (52.07%)	179 (82.49%)	137 (63.13%)	154 (70.97%)	207 (95.39%)

Table 5
Error range distribution for all data.

Error range (%)	Number of data and corresponding percentage in the error range					
	EC 4	AISC 360–16	ASNZS 2327	Wang et al. [62]	Tran et al. [63]	*GTB*
± 5	315	117	327	241	211	920
	(30.97%)	(11.50%)	(32.15%)	(23.70%)	(22.75%)	(90.46%)
± 10	557	218	576	432	448	980
	(54.77%)	(21.44%)	(56.64%)	(42.48%)	(46.05%)	(96.36%)
± 15	733	396	732	566	609	995
	(72.07%)	(38.94%)	(71.98%)	(55.65%)	(59.88%)	(97.84%)
± 20	859	567	860	692	736	1006
	(84.46%)	(55.75%)	(84.56%)	(68.04%)	(72.37%)	(98.92%)

References

[1] Reich Y. Machine learning techniques for civil engineering problems. Comput-Aided Civ Infrastruct Eng 1997;12(4):295–310.

[2] MELHEM HANIG, NAGARAJA SRINATH. Machine learning and its application to civil engineering systems. Civil Eng Syst 1996;13(4):259–79.

[3] Huang Y, Li J, Fu J. Review on application of artificial intelligence in civil engineering. Comput Model Eng Sci 2019;121:845–75.

[4] Salehi H, Burgueño R. Emerging artificial intelligence methods in structural engineering. Eng Struct 2018;171:170–89.

[5] Lee S, Ha J, Zokhirova M, Moon H, Lee J. Background information of deep learning for structural engineering. Arch Comput Methods Eng 2018;25(1):121–9.

[6] Lee S, Kim H, Lieu QX, Lee J. CNN-based image recognition for topology optimization. Knowl-Based Syst 2020;198:105887. https://doi.org/10.1016/j.knosys.2020.105887.

[7] Truong TT, Lee S, Lee J. An artificial neural network-differential evolution approach for optimization of bidirectional functionally graded beams. Compos Struct 2020;233:111517. https://doi.org/10.1016/j.compstruct.2019.111517.

[8] Lee S, Zokhirova M, Nguyen TT, Lee J. Effect of hyper-parameters on deep learning networks in structural engineering. In: Proceedings of the International Conference on Advances in Computational Mechanics (ACOME); 2017, pp. 537–44.

[9] Nguyen TN, Lee S, Nguyen-Xuan H, Lee J. A novel analysis-prediction approach for geometrically nonlinear problems using group method of data handling. Comput Methods Appl Mech Eng 2019;354:506–26.

[10] Bui D-K, Nguyen T, Chou J-S, Nguyen-Xuan H, Ngo TD. A modified firefly algorithm-artificial neural network expert system for predicting compressive and tensile strength of high-performance concrete. Constr Build Mater 2018;180:320–33.

[11] Yeh I-C. Modeling of strength of high-performance concrete using artificial neural networks. Cem Concr Res 1998;28(12):1797–808.

[12] Noorzaei J, Hakim S, Jaafar M, Thanoon W, Technology. Development of artificial neural networks for predicting concrete compressive strength. Int J Eng Technol 2007;4:141–53.

[13] Naderpour H, Rafiean AH, Fakharian P. Compressive strength prediction of environmentally friendly concrete using artificial neural networks. J Build Eng 2018;16:213–9.

[14] Anghelescu L, Cruceru M, Diaconu B. Building materials obtained by recycling coal ash and waste drilling fluid and characterization of engineering properties by means of Artificial Neural Networks. Constr Build Mater 2019;227:116616. https://doi.org/10.1016/j.conbuildmat.2019.07.342.

[15] Sadati S, Silva LEBd, Wunsch DC, Khayat KH. Artificial intelligence to investigate modulus of elasticity of recycled aggregate concrete. ACI Mater J 2019;116:51–62.

[16] Getahun MA, Shitote SM, Abiero Gariy ZC. Artificial neural network based modelling approach for strength prediction of concrete incorporating agricultural and construction wastes. Constr Build Mater 2018;190:517–25.

[17] Tenza-Abril AJ, Villacampa Y, Solak AM, Baeza-Brotons F. Prediction and sensitivity analysis of compressive strength in segregated lightweight concrete based on artificial neural network using ultrasonic pulse velocity. Constr Build Mater 2018;189:1173–83.

[18] Onyari EK, Ikotun BD. Prediction of compressive and flexural strengths of a modified zeolite additive mortar using artificial neural network. Constr Build Mater 2018;187:1232–41.

[19] Behnood A, Golafshani EM. Predicting the compressive strength of silica fume concrete using hybrid artificial neural network with multi-objective grey wolves. J Cleaner Prod 2018;202:54–64.

[20] Naser MZ. Properties and material models for modern construction materials at elevated temperatures. Comput Mater Sci 2019;160:16–29.

[21] Naser MZ. Fire resistance evaluation through artificial intelligence - A case for timber structures. Fire Saf J 2019;105:1–18.

[22] Naser MZ. Heuristic machine cognition to predict fire-induced spalling and fire resistance of concrete structures. Autom Constr 2019;106:102916. https://doi.org/10.1016/j.autcon.2019.102916.

[23] Naser MZ. AI-based cognitive framework for evaluating response of concrete structures in extreme conditions. Eng Appl Artif Intell 2019;81:437–49.

[24] Naser MZ, Kodur VKR. Cognitive infrastructure - a modern concept for resilient performance under extreme events. Autom Constr 2018;90:253–64.

[25] Naser MZ. Deriving temperature-dependent material models for structural steel through artificial intelligence. Constr Build Mater 2018;191:56–68.

[26] Abbas H, Al-Salloum YA, Elsanadedy HM, Almusallam TH. ANN models for prediction of residual strength of HSC after exposure to elevated temperature. Fire Saf J 2019;106:13–28.

[27] Liu J-C, Zhang Z. Neural network models to predict explosive spalling of PP fiber reinforced concrete under heating. J Build Eng 2020;32:101472. https://doi.org/10.1016/j.jobe.2020.101472.

[28] Akbarzadeh Bengar H, Shahmansouri AA, Akkas Zangebari Sabet N, Kabirifar K, W.Y. Tam V. Impact of elevated temperatures on the structural performance of recycled rubber concrete: experimental and mathematical modeling. Constr Build Mater 2020;255:119374.

[29] Naser MZ, Uppala VA. Properties and material models for construction materials post exposure to elevated temperatures. Mech Mater 2020;142:103293. https://doi.org/10.1016/j.mechmat.2019.103293.

[30] Zhou Y, Zheng S, Huang Z, Sui L, Chen Y. Explicit neural network model for predicting FRP-concrete interfacial bond strength based on a large database. Compos Struct 2020;240:111998. https://doi.org/10.1016/j.compstruct.2020.111998.

[31] Abambres M, Lantsoght EOL. Neural network-based formula for shear capacity prediction of one-way slabs under concentrated loads. Eng Struct 2020;211:110501. https://doi.org/10.1016/j.engstruct.2020.110501.

[32] Erdem H. Prediction of the moment capacity of reinforced concrete slabs in fire using artificial neural networks. Adv Eng Softw 2010;41(2):270–6.

[33] Al-Khaleefi AM, Terro MJ, Alex AP, Wang Y. Prediction of fire resistance of concrete filled tubular steel columns using neural networks. Fire Saf J 2002;37(4):339–52.

[34] Tran V-L, Thai D-K, Nguyen D-D. Practical artificial neural network tool for predicting the axial compression capacity of circular concrete-filled steel tube columns with ultra-high-strength concrete. Thin-Walled Struct 2020;151:106720. https://doi.org/10.1016/j.tws.2020.106720.

[35] Tran V-L, Kim S-E. Efficiency of three advanced data-driven models for predicting axial compression capacity of CFDST columns. Thin-Walled Struct 2020;152:106744. https://doi.org/10.1016/j.tws.2020.106744.

[36] Tran V-L, Thai D-K, Kim S-E. Application of ANN in predicting ACC of SCFST column. Compos Struct 2019;228:111332. https://doi.org/10.1016/j.compstruct.2019.111332.

[37] Nguyen HQ, Ly H-B, Tran VQ, Nguyen T-A, Le T-T, Pham BT. Optimization of artificial intelligence system by evolutionary algorithm for prediction of axial capacity of rectangular concrete filled steel tubes under compression. Materials 2020;13:1205.

[38] Ahmadi M, Naderpour H, Kheyroddin A. Utilization of artificial neural networks to prediction of the capacity of CCFT short columns subject to short term axial load. Arch Civil Mech Eng 2014;14(3):510–7.

[39] Ahmadi M, Naderpour H, Kheyroddin A. ANN model for predicting the compressive strength of circular steel-confined concrete. Int J Civil Eng 2017;15(2):213–21.

[40] Du Y, Chen Z, Zhang C, Cao X. Research on axial bearing capacity of rectangular concrete-filled steel tubular columns based on artificial neural networks. Front Comput Sci 2017;11(5):863–73.

[41] Jiang K, Han Q, Bai Y, Du X. Data-driven ultimate conditions prediction and stress-strain model for FRP-confined concrete. Compos Struct 2020;242:112094. https://doi.org/10.1016/j.compstruct.2020.112094.

[42] Djerrad A, Fan F, Zhi X-d, Wu Q-j. Artificial neural networks (ANN) based compressive strength prediction of AFRP strengthened steel tube. Int J Steel Struct 2020;20:156–74.

[43] Naderpour H, Nagai K, Fakharian P, Haji M. Innovative models for prediction of compressive strength of FRP-confined circular reinforced concrete columns using soft computing methods. Compos Struct 2019;215:69–84.

[44] Ren Q, Li M, Zhang M, Shen Y, Si W. Prediction of ultimate axial capacity of square concrete-filled steel tubular short columns using a hybrid intelligent algorithm. Appl Sci 2019;9:2802.

[45] Cascardi A, Micelli F, Aiello MA. An Artificial Neural Networks model for the prediction of the compressive strength of FRP-confined concrete circular columns. Eng Struct 2017;140:199–208.

[46] Hung TV, Viet VQ, Van Thuat D. A deep learning-based procedure for estimation of ultimate load carrying of steel trusses using advanced analysis. J Sci Technol Civil Eng 2019;13:113–23.

[47] Truong V-H, Vu Q-V, Thai H-T, Ha M-H. A robust method for safety evaluation of steel trusses using Gradient Tree Boosting algorithm. Adv Eng Softw 2020;147:102825. https://doi.org/10.1016/j.advengsoft.2020.102825.

[48] Duan J, Asteris PG, Nguyen H, Bui X-N, Moayedi H. A novel artificial intelligence technique to predict compressive strength of recycled aggregate concrete using ICA-XGBoost model. Eng Comput 2020.

[49] Nguyen-Sy T, Wakim J, To Q-D, Vu M-N, Nguyen T-D, Nguyen T-T. Predicting the compressive strength of concrete from its compositions and age using the extreme gradient boosting method. Constr Build Mater 2020;260:119757. https://doi.org/10.1016/j.conbuildmat.2020.119757.

[50] Feng D-C, Liu Z-T, Wang X-D, Chen Y, Chang J-Q, Wei D-F, et al. Machine learning-based compressive strength prediction for concrete: an adaptive boosting approach. Constr Build Mater 2020;230:117000. https://doi.org/10.1016/j.conbuildmat.2019.117000.

[51] Morino S, Uchikoshi M, Yamaguchi I. Concrete-filled steel tube column system-its advantages. Steel Struct 2001;1:33–44.

[52] Liew JYR, Xiong M, Xiong D. Design of concrete filled tubular beam-columns with high strength steel and concrete. Structures 2016;8:213–26.

[53] Uy B. Concrete-filled fabricated steel box columns for multistorey buildings: behaviour and design. Prog Struct Mat Eng 1998;1(2):150–8.

[54] Thai H-T, Uy B, Khan M, Tao Z, Mashiri F. Numerical modelling of concrete-filled steel box columns incorporating high strength materials. J Constr Steel Res 2014;102:256–65.

[55] EN1994-1-1. Eurocode 4: Design of composite steel and concrete structures - Part 1-1: General rules and rules for buildings; 2004.

[56] BS5400-5. Steel, concrete and composite bridges. Code of practice for design of composite bridges. British Standards Institute (BSI); 2005.

[57] AISC 360-16. Specification for structural steel buildings; 2016.

[58] GB 50936. Technical code for concrete-filled steel tubular structures. China National Standards; 2014.

[59] Architectural Institute of Japan (AIJ). Recommendations for design and construction of concrete filled steel tubular structures, Japan; 1997.

[60] Standards Australia. AS/NZS 2327 Composite structures - Composite steel-concrete construction in buildings; 2017.

[61] Azmee NM, Shafiq N. Ultra-high performance concrete: from fundamental to applications. Case Stud Constr Mater 2018;9:e00197. https://doi.org/10.1016/j.cscm.2018.e00197.

[62] Wang Z-B, Tao Z, Han L-H, Uy B, Lam D, Kang W-H. Strength, stiffness and ductility of concrete-filled steel columns under axial compression. Eng Struct 2017;135:209–21.

[63] Tran V-L, Thai D-K, Kim S-E. A new empirical formula for prediction of the axial compression capacity of CCFT columns. Steel Compos Struct 2019;33:181–94.

[64] Thai S, Thai H-T, Uy B, Ngo T. Concrete-filled steel tubular columns: test database, design and calibration. J Constr Steel Res 2019;157:161–81.

[65] Thai S, Thai H-T, Uy B, Ngo T, Naser MZ. Test database on concrete-filled steel tubular columns. Mendeley Data 2019. https://doi.org/10.17632/3xknb3sdb5.2.

[66] Friedman JH. Greedy function approximation: a gradient boosting machine. Ann Stat 2001;29(5):1189–232.